

Integration of Crystal Morphology Modeling and On-Line Shape Measurement

R. F. Li, G. B. Thomson, and G. White

School of Engineering and Physical Sciences, Heriot-Watt University, Edinburgh EH14 4AS, U.K.

X. Z. Wang, J. Calderon De Anda, and K. J. Roberts

Institute of Particle Science and Engineering, School of Process, Environmental and Materials Engineering, University of Leeds, Leeds LS2 9JT, U.K.

DOI 10.1002/aic.10818

Published online April 5, 2006 in Wiley InterScience (www.interscience.wiley.com).

Introduction

The shape of pharmaceutical crystals grown from solution is known to have an important effect on the end-use functional properties and downstream processing, and handling of the product. Significant progress has been made in recent years in both crystal morphology modeling and shape measurement using on-line imaging techniques. The current investigation of an approach for integrating both techniques is motivated by the prospect that such integration can lead to a useful instrument for validating morphology prediction models, for constructing 3-D shapes from 2-D on-line images, as well as for the potential of obtaining crystal size and growth rates of individual facets of a 3-D crystal.

Early morphological modeling techniques were based on Bravais-Freidel-Donnay-Harker (BFDH) law and Hartman-Perdok's periodic bond chain (PBC) theory.¹ The BFDH law states that, allowing for submultiples of the interplanar spacing due to space group symmetry (that is, centering, screw axes, glide planes), the most important crystallographic forms have the greatest interplanar spacing. The law related the external crystal shape to the internal crystallographic structure, which is still useful for quickly identifying the likely growth faces. The PBC theory extended the idea inherent in the BFDH law by considering the strength and stoichiometry of the solid-state intermolecular forces involved in the crystallization process, in particular through calculation of the surface attachment energy, that is, the energy released on the addition of a building unit to the surface of a growing crystal which is taken as a measure of the relative growth rate of that face. The methods implement-

ing these theories and resulting developments are now well established and reliable software tools are now available. These methods have been widely and successfully used to predict the crystal shape of organic compounds such as pharmaceuticals,²⁻¹⁰ and been implemented in computer programs, such as HABIT^{11,12} Cerius2¹³, and MORANG¹⁴. A major limitation of these methods is that they have only taken into consideration of the internal structure information of the crystal, such as unit cell parameters, fractional coordinates and symmetry information, but have largely ignored the effects of process operating conditions, such as supersaturation, cooling rates, solvents, impurities or additives.

New approaches have been proposed in the past 10 years that use modified Hartman and Perdok's attachment energy,^{15,16} detailed kinetics principles,¹⁷⁻²¹ and Monte Carlo techniques^{22,23} with the attempts to incorporate the effect of solvents, additives, supersaturation and cooling rates into crystal morphology prediction models. Clydesdale et al.^{15,16} used modified Hartman and Perdok's attachment energy to model the crystal morphology in the presence of blocking tailor-made and disruptive tailor-made additives. Bennema's group have used detailed crystal growth kinetics as means of predicting crystal morphology grown from solution.^{17,24,25} In their method, the kinetic models are simplified to retain only one solvent dependent parameter which can be derived from computer simulation of the solid-fluid interaction. Doherty's group developed a similar approach based on the detailed crystal growth kinetics¹⁸⁻²¹ through a method which requires only a calculation of the nature of the intermolecular interactions along the different growth directions, rather than complex simulation. Monte Carlo simulation was also investigated by Boerrigter et al.²² with the aim of incorporating the effect of supersaturation on crystal morphology modeling and more recently, Gadewar and Doherty²⁶ developed a dynamic model that allows for the

Correspondence concerning this article should be addressed to X. Z. Wang at x.z.wang@leeds.ac.uk.

prediction of the shape evolution of 2-D crystals from arbitrary initial shapes. This model not only can account for faces appearing and disappearing during the evolution, but also can predict the crystal shape at steady state. Comprehensive review of the literature on morphological modeling has been made by Winn and Doherty²⁷, Rohl²⁸, Clydesdale et al.⁸⁻¹⁰

Another important area for crystal shape investigation is its on-line measurement. Although it has been mainly aimed at real-time monitoring and control, in principle, could be used for validation of modeling techniques. Laser diffraction^{29,30} and ultrasound³¹ have been investigated for this purpose, but the most promising technique seems to be on-line microscopy imaging. Patience and Rawlings^{32,33} studied the use of the Lasentec³⁴⁻³⁶ particle vision measurement (PVM) system together with a stop-flow-cell system for measuring crystal shapes on-line. In a previous study, Calderon De Anda et al.³⁷⁻⁴¹ reported the use of an on-line imaging system developed by the pharmaceutical company GlaxoSmithKline for monitoring polymorph transitions and crystallization on-set. Calderon De Anda et al.³⁹ also developed an effective multiscale approach for the image analysis of in-process data, as well as a method for classification of crystal polymorphic and morphological forms.⁴¹

The purpose of this article is to present the *camera model* — a new approach for integrating both crystal morphological modeling and on-line shape measurement techniques. The communication is organized as follows. In the next section, the overall framework of the proposed methodology will be presented. The details of the methodology, that is, the camera model, the 2-D shape descriptors, and the approach for rotating the 3-D crystal in order to generate 2-D projections, will be described in the Camera Model and Shape Descriptor section. A case study using the proposed method for real time recognition of crystal polymorphs will be discussed in the Case Study: Crystallization of the α and β Forms of (L)-Glutamic Acid section, and the final remarks will be made in the last section.

Framework

The overall framework for integrating shape modeling and measurement is summarized in Figure 1. It consists of five component modules: morphological modeling for predicting 3-D shapes; 3-D shape rotation and use of a camera model for projecting a 3-D crystal to a library of 2-D images; real 2-D images acquisition from on-line imaging instrument; on-line image analysis; and matching between images in the library and the processed on-line images.

The top-left dashed box is the component for 3-D shape generation using morphological modeling. As reviewed in the first section that although early methods and software, such as Cerius2¹³, Habit^{11,12,15}, and MORANG¹⁴ only considered crystal internal structure information, progress is being made to consider engineering operational conditions including supersaturation, solvents, additives and cooling rates.¹⁸⁻²² In addition, although not included in Figure 1, other experimental techniques for crystal shape determination can also be used, such as the high-throughput technique, which can simultaneously conduct hundreds of experiments under different operating conditions and has been used in polymorphic screening.⁴²

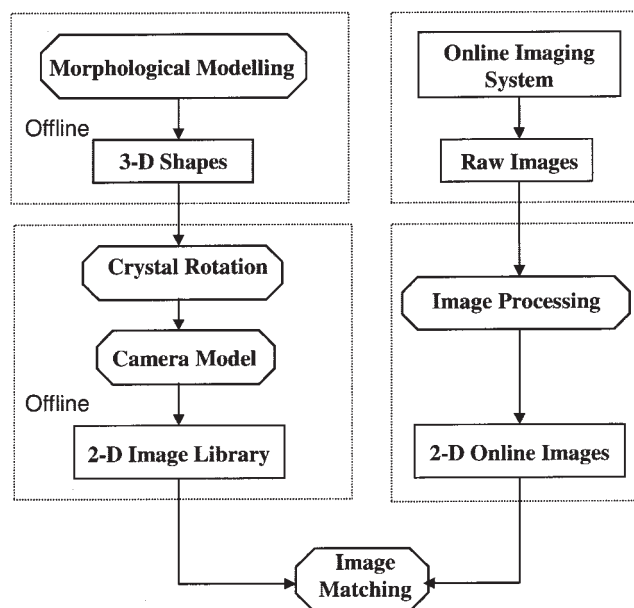


Figure 1. Proposed framework for the integration of morphology modeling and on-line shape measurement using the digital video microscopy system

The bottom left dashed box is the step to project a 3-D crystal shape to 2-D images through rotating the crystal in the multidimensional space and using the *camera model*. Although in order to provide a credible 2-D image library of an arbitrary shaped object the necessary rotation angles can be indefinite, for a crystal that has a structured shape, the rotation angles needed can be estimated, as will be demonstrated in the next section.

The two dashed boxes on the righthand side of Figure 1 are raw image acquisition from reactors using on-line imaging instrument, and image processing for the purpose of extracting objects from the background of an image and for removing noises.

The bottom box is the step to calculate the shape descriptors and the similarity distances between the 2-D images in the library and obtained on-line.

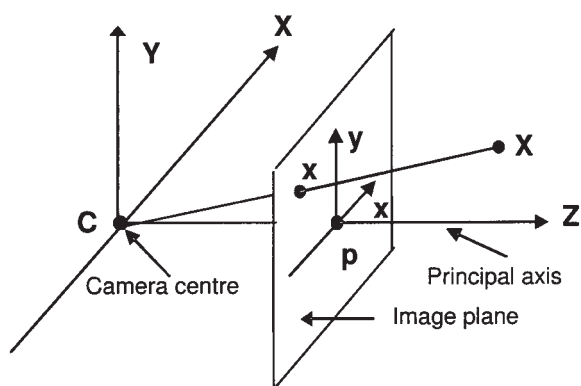
Camera Model and Shape Descriptor

Camera model

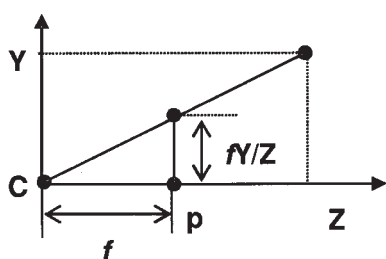
Recording images using a camera model is equivalent to mapping an object point in the object space to an image point in the image space.⁴³ The camera model (also known as the pinhole camera model) can be illustrated using Figure 2. Under the pinhole camera model, a point in the object space with coordinates $\mathbf{X} = (X, Y, Z)^T$ is mapped to a point \mathbf{x} with coordinates $(fX/Z, fY/Z, f)^T$ on the image plane. The mapping can be written as

$$(X, Y, Z)^T \leftrightarrow (fX/Z, fY/Z)^T \quad (1)$$

On the above projection, the camera position is called the camera center. The line from the camera center perpendicular



(a)



(b)

Figure 2. Basic principles underpinning the pinhole camera model, (a) the basic concepts, and (b) the projection geometrics.⁴⁵

to the image plane is called the principal axis, and the point where the principal axis meets the image plane is called the principal point. If the object and image points are represented by homogeneous vectors, the above projection is very simply expressed as a linear mapping between their homogeneous coordinates. In particular, Eq. 1 can be written in terms of matrix multiplication as

$$\begin{pmatrix} X \\ Y \\ Z \\ 1 \end{pmatrix} \rightarrow \begin{pmatrix} fX \\ fY \\ Z \end{pmatrix} = \begin{bmatrix} f & 0 & 0 \\ 0 & f & 0 \\ 0 & 0 & 1 \end{bmatrix} \begin{pmatrix} X \\ Y \\ Z \\ 1 \end{pmatrix} \quad (2)$$

In the real situation, the relationship between 3-D world point and image point can be more complex than the above equation. We have to consider some more situations, such as when the origin of the image coordinate system is not principal point p , the object coordinate system is different from the camera coordinate, the image coordinates are measured in pixels, and distortion of camera lens. The general expression of the camera model can be written as

$$\begin{pmatrix} x \\ y \\ z \end{pmatrix} = \begin{pmatrix} p_{11} & p_{12} & p_{13} & p_{14} \\ p_{21} & p_{22} & p_{23} & p_{24} \\ p_{31} & p_{32} & p_{33} & p_{34} \end{pmatrix} \begin{pmatrix} X \\ Y \\ Z \\ 1 \end{pmatrix} = P \begin{pmatrix} X \\ Y \\ Z \\ 1 \end{pmatrix} \quad (3)$$

where the matrix P is called calibration matrix of the camera, which includes the internal and external parameters of the camera. These parameters can be determined by camera calibration. Camera calibration is usually to design a calibration object whose geometry in the 3-D space is known, then uses the point correspondences between 3-D points and 2-D image points to determine the camera parameters. However, in our system, the camera model is only used to transform the 3-D object to 2-D images. In this case, we are only concerned with the 2-D projection onto a plane of the 3-D polyhedral shape. Therefore, we can design a camera system where the origin of image coordinate system is principal point p , the object coordinate system is the same as the camera coordinates, and distortion of camera lens can be ignored. In this way, we can directly use Eq. 2 as the camera model. The parameters f in Eq. 2 can be freely chosen because it only affects the size of the transformed image. In this work we used such a camera system where the coordinates of a crystal can be obtained by crystal rotation.

Shape descriptors

A number of techniques have been proposed in recent years to use descriptors to represent the shape of an object. These techniques can be generally categorized into two classes: contour-based and region-based methods. The details of the methods can be found in a recent review article.⁴⁴

In this work, Fourier descriptors were used to extract features from the crystal 2-D shapes. Fourier descriptors can be obtained by applying the Fourier transform on shape boundary signatures, such as curvature, radius and complex coordinates. It is found that shape classification performances based on these three signatures do not differ significantly.⁴⁵ In our system, we used radius-based signature, mainly because it is the simplest to implement.

Radius-based signature consists of a number of ordered distances from the shape centroid to boundary points (called *radii*), as shown in Figure 3.

$$r_i = \sqrt{(x_i - x_c)^2 + (y_i - y_c)^2} \quad (i = 0, 1, 2 \dots N - 1) \quad (4)$$

Where r_i is the distance from the shape centroid (x_c, y_c) to the i^{th} boundary sampling point (x_i, y_i) , N is the number of the sampling points. In our system, 64 uniformly sampled boundary points and, thus, 64 ordered radii are used as shape signa-

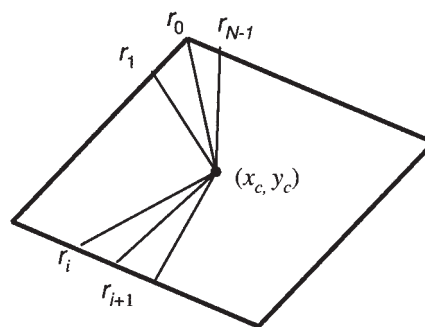


Figure 3. Definition of the radius-based shape signature used in the shape analysis.

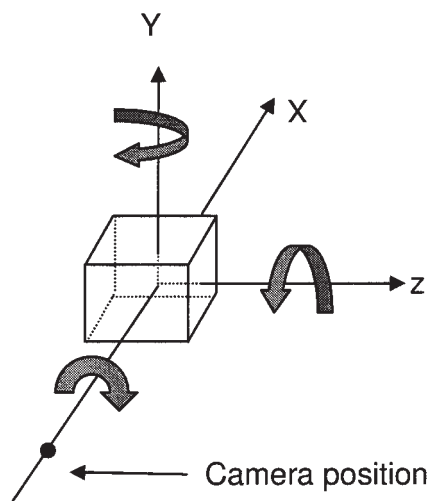


Figure 4. Axial conventions used for the crystal rotation method.

ture. The boundary points are sampled such that the number of pixels along the boundary between each two neighboring points is the same. The Fourier descriptors (FD) based on the shape radii are then given by

$$F_n = \frac{1}{N} \sum_{i=0}^{N-1} r_i \exp\left(\frac{-j2\pi ni}{N}\right), \quad n = 0, 1, \dots, N-1 \quad (5)$$

The FDs acquired in this way is translation invariant due to the translation invariance of the shape radii. The orientation invariance is achieved by ignoring the phase information of FDs. We only use the absolute value of the descriptors, that is, $|F_n|$, is invariant to rotation. $|F_0|$ reflects the average value of the shape radii, which is dependent on the scale of the shape, thus $|F_n|/|F_0|$ will be scale invariant. Since the centroid distance is a real value function, only half of the FDs are needed. The final Fourier descriptors can be expressed as

$$FD_k = |F_k|/|F_0|, \quad k = 1, 2, \dots, N/2. \quad (6)$$

In the descriptors, the low-frequency descriptors contain information about the general shape, and the higher frequency descriptors contain information about smaller details.

The Fourier-descriptor based similarity distance can be expressed as

$$d_{sim} = \left(\sum_{i=1}^L (FD_{1,i} - FD_{2,i})^2 \right)^{1/2} \quad (7)$$

where $FD_{1,i}$ $FD_{2,i}$ is the i^{th} Fourier descriptor of the images 1 and 2, respectively, L is the number of the Fourier descriptors

used to represent the shape. The smaller the similarity distance, the more similar the two images.

Crystal rotation

The method for rotating a 3-D crystal in order to produce any possible 2-D projections using a camera model is illustrated in Figure 4. If the camera is placed at a point on the **X** axis, as shown in Figure 4, the rotation around **X** axis will not result in different 2-D shapes, but only change the orientations of the same 2-D shape. As a result, the rotation around **X** axis can be ignored. Since the crystal is a faceted object, when rotating around an axis, either **Y**, or **Z**, from one angle to another at a very small step, for example around **Y** axis, the 2-D shapes corresponding to the two positions may only change very little. Figure 5 shows some 2-D shapes when rotating a crystal at different angles from a position, 1°, 2°, 3°, 4°, 5°, 6°, 7°, 8°, 9°, 10°, and 11° around **Z** axis, from which it is clear that even when rotating the crystal 11° from the initial position, the 2-D shape does not change very much. This means that the number of 2-D shapes having significant difference with each other is limited. Here the words “significant difference” although are vague, can be defined by the users. For instance, it can be defined as that as long as the number of edges in the projected 2-D images changes (increases or decreases), then it is considered as a new 2-D image that has significant difference from its last image. It is worth pointing out that the minimum degree at which the crystal needs to rotate is dependent on the complexity of the 3-D crystal and the initial position of rotation.

Two possible methods of rotation are proposed here but only one is used in this study. The first approach is to use a fixed rotation angle to continuously rotate the crystal. In this case, the value of the angle must be small enough so that the similarity distance between two 2-D shapes corresponding to any two neighboring orientations is smaller than a predefined threshold value. The detailed steps of this rotation are described below:

1. Let $i = 1$, read the initial orientation data;
2. From the initial orientation, rotate the crystal ($i \times \theta$) ($i = 1, 2, 3, \dots, M$) degree around the **Z** axis, respectively. This will produce **M** new orientations.

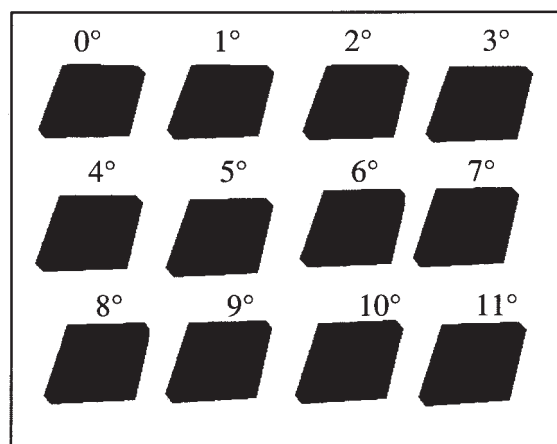
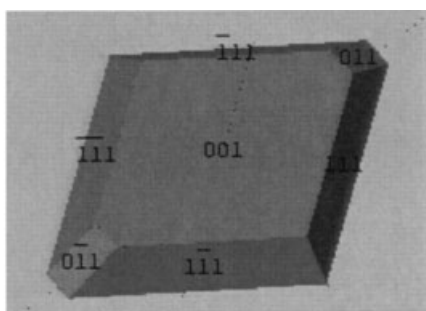
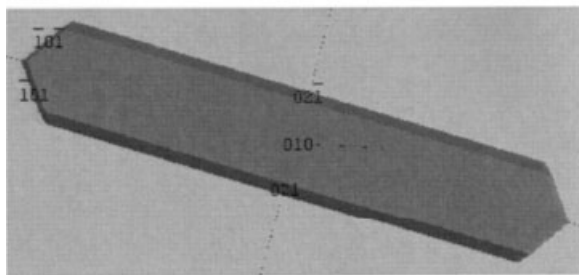


Figure 5. Projected 2-D shapes from 3-D onto a plane following rotation at different angles.



(a)



(b)

Figure 6. Predicted crystal morphologies for (L)-glutamic acid based on attachment energy calculations, (a) α - form, (b) β - form.

3. From each of \mathbf{M} new orientations, rotate the crystal, ($j \times \phi$) ($j = 1, 2, 3, \dots, \mathbf{N}$) degree around the \mathbf{Y} axis, respectively.

where, θ, ϕ are the step rotation angles around \mathbf{Z} and \mathbf{Y} axes, respectively, then $\mathbf{M} = 360/\theta$ and $\mathbf{N} = 360/\phi$ are the rotation times around \mathbf{Z} and \mathbf{Y} axes, respectively. The number of total orientations based on the above steps is $\mathbf{M} \times \mathbf{N}$, which means that each 3-D crystal will have $\mathbf{M} \times \mathbf{N}$ projected 2-D images in the library.

An alternative approach of rotation is to use variant rotation angles. In this approach, when rotating the crystal around an axis from one position to the next position, the angle between the two is chosen so that the similarity distance of the two 2-D shapes corresponding to the two positions is larger than a threshold value sd_1 and smaller than another threshold value sd_2 ($sd_1 < sd_2$). The advantage of this rotation method is that it can reduce the size of the 2-D image library generated.

In this study, only the first approach, that is, the fixed rotation angle method is used, which produces $\mathbf{M} \times \mathbf{N}$ orientations of a crystal. The 3-D crystal at these $\mathbf{M} \times \mathbf{N}$ orientations is then transformed into $\mathbf{M} \times \mathbf{N}$ 2-D shapes using the camera model. For each of these transformed 2-D shapes, the Fourier descriptors are calculated, which are stored in an image database for future matching with online images. In the database, each set of FDs represents a 2-D shape of the crystal at an orientation. When online images become available, the FDs of the online images will be first calculated. Then the most similar 2-D shapes with the online image in the database will be retrieved through calculating the similarity distance between the online image and database images.

Case Study: Crystallization of the α and β Forms of (L)-Glutamic Acid

In this section, we apply the method for real-time recognition of the polymorphs of (L)-glutamic acid during its batch cooling crystallization from supersaturated aqueous solution. Although there are established techniques for on-line identification of crystal polymorphs such as X-ray diffraction and Raman spectroscopy,⁴⁶ here the purpose is mainly to exemplify the use of integration of crystal morphology modeling and shape measurement and the associated utility of this approach for following crystal growth and polymorphic transformation processes.

Morphological prediction from the crystallographic data

(L)-glutamic acid has two known polymorphs: the prismatic α and needle-like β forms. The crystal structure of the α -form has space group symmetry $P2_12_12_1$ with four molecules in the unit cell ($a = 7.068 \text{ \AA}$, $b = 10.277 \text{ \AA}$, $c = 8.755 \text{ \AA}$, $\alpha = \beta = \gamma = 90^\circ$)⁴⁷, the β -form belongs to the same space group but has different parameters of the unit cell ($a = 5.159 \text{ \AA}$, $b = 17.34 \text{ \AA}$, $c = 6.948 \text{ \AA}$, $\alpha = \beta = \gamma = 90^\circ$)⁴⁸. The detailed structure information of these two forms can be obtained from the Chemical Database Services.⁴⁹ Based on the 3-D crystallographic structure information of the two forms of (L)-glutamic acid, these morphologies were predicted using a range of computer morphology simulation software packages including Cerius2¹³, MOPAC⁵⁰, HABIT^{11,12}, and SHAPE⁵¹. In this approach, Cerius2 was used to generate the basic symmetry information of the crystals and via the BFDH rules produce a list of the likely low-index growth faces and MOPAC was used to calculate the partial atomic charges. The attachment energies for the selected growth faces was obtained using HABIT from which the morphology of the crystal was simulated by setting the relative crystal growth rate to be proportional to the surface attachment energy using the program SHAPE. Background

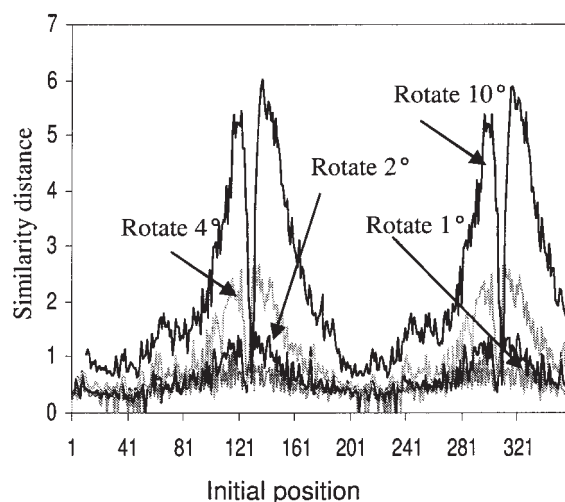
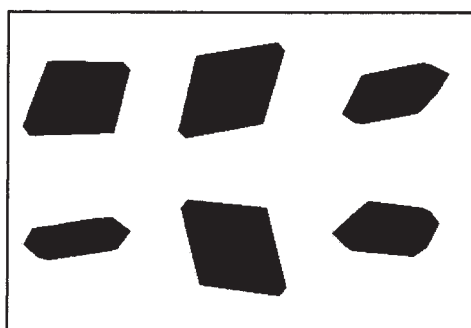
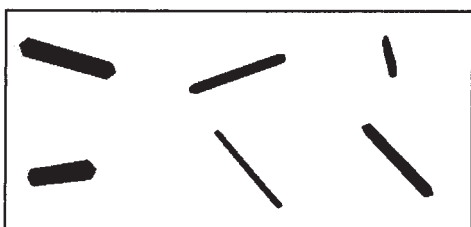


Figure 7. Comparison of the similarity distances between the original and rotated images at different rotation angles and different initial positions.



(a)



(b)

Figure 8. Some 2-D projected image examples of (L)-glutamic acid crystal in the generated image library, (a) α - form, (b) β -form.

articles together with more details of the procedures adopted for predicting the crystal morphology using this approach can be found in the references.^{9, 10, 12} Figure 6 shows an example of the resultant predicted 3-D shapes of the α and β forms, revealing the α form to be dominated by the (001) face, and the β form to be dominated by the (010) face.

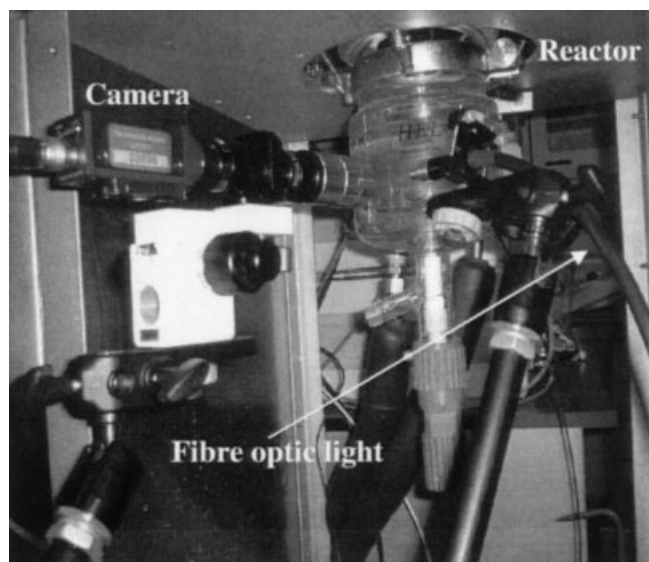
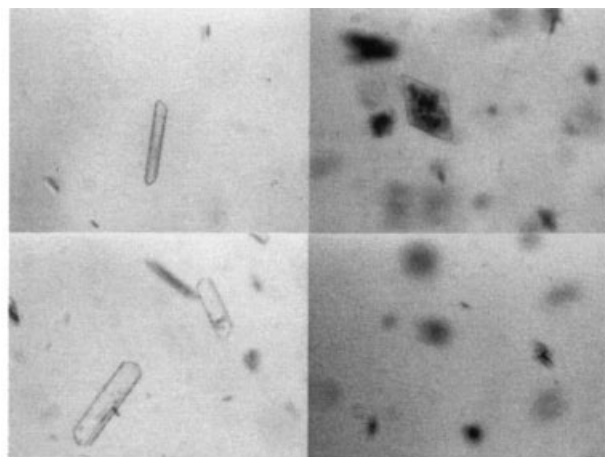


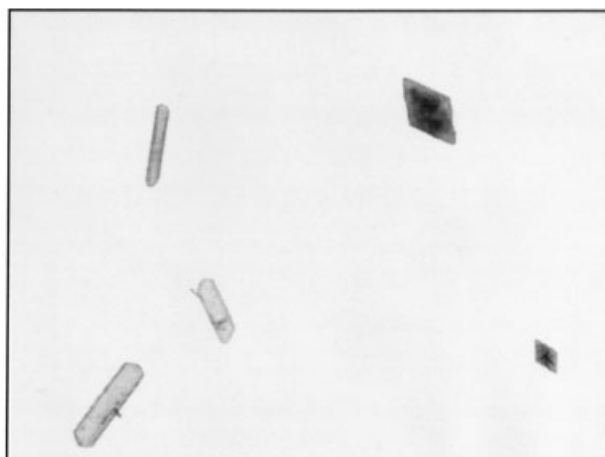
Figure 9. Experimental setup comprising automated 500 mL batch reactor equipped with the on-line digital video microscopy system.⁴⁰

2-D image library generation through rotating 3-D crystals

The extraction of the 2-D projected perimeter maps from the rotation of the predicted 3-D shapes can be illustrated using the distinctive morphologies of the α and β forms of (L)-glutamic acid. The key parameter in crystal rotation is the rotation angle, which is the angle between the two neighboring orientations. A large rotation angle can result in loss of information, but a small angle can lead to an unreasonably large size for the image library. In practice, trial-and-error methods can be used to determine an appropriate interval for the angular rotation. This approach is demonstrated in Figure 7 which shows the similarity distance between the original and rotated images of the α form of (L)glutamic acid when rotating the crystal shape by different angles of 1°, 2°, 4°, and 10°, respectively, from different orientations. From this Figure, we can see that larger angles give larger similarity distance between the original and








(a)



(b)

Figure 10. Four on-line images of (L)-glutamic acid taken with digital video microscopy system, (a) raw images, and (b) segmented images.

Table 1. The Image Matching Result for Images in Figure 10

Online Images	Retrieved Image Reference	Similarity Distance	Polymorph
	BetaM042182	1.40	β
	BetaM112182	1.44	β
	BetaM112358	1.48	β
	BetaM280330	0.88	β
	BetaM104030	0.89	β
	BetaM284330	0.96	β
	AlphaM176054	0.87	α
	AlphaM356126	0.88	α
	AlphaM176234	0.88	α
	BetaM022228	0.46	β
	BetaM022048	0.51	β
	BetaM320134	0.52	β
	AlphaM356018	0.65	α
	AlphaM354198	0.68	α
	AlphaM004016	0.68	α

rotated shapes. 4° and 10° give larger distance, and the library size when rotation angle is 1° will become very large, thus, 2° is a suitable choice.

When the rotation angle is 2° , the size of the image library produced by the α and β forms of Figure 6 is $2 \times 180 \times 180$. The calculated Fourier descriptors for the library images are stored in a database. Some examples of the 2-D library image are shown in Figure 8.

On-line image processing and recognition of polymorphs

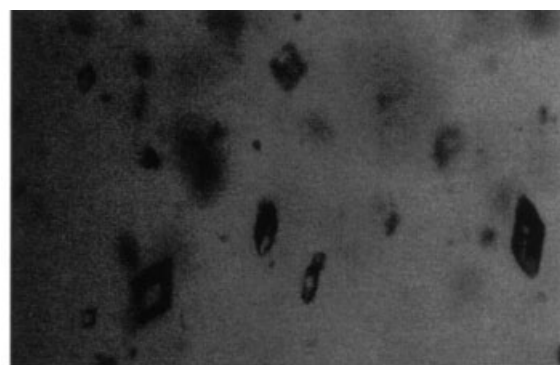
The on-line imaging system employed in our study was developed by GlaxoSmithKline (GSK).^{52, 53} Figure 9 shows a snapshot of the imaging system. A CCD camera fitted with Navitar Precise Eye/Mitutoyo optics is employed for image acquisition with a maximum frequency of up to thirty images per second with a pixel resolution of 640×480 , and a field of view from $140 \mu\text{m}$ to 16mm dependent on calibration lenses employed. The camera was situated just outside the reactor wall and an image window was attached to the external reactor wall to minimize convexity effects on the images. To provide illumination, a xenon strobe light source was used with the light being conducted using a fiber optic guide. Camera acquisition and strobe are synchronised to freeze the moving particles by using a camera interface box developed by GSK. The captured images are sent to a PC running Video Savant® software⁵⁴ for acquisition, storage and management of frames. To enhance the contrast of particles from image background, two fiber optic light guides can also be used, both adjustable in angles and distances from the camera. The overall system allows the capability to visualize and record in real-time every

event occurring throughout the complete batch crystallization run. In an early report we have used this instrument as set-up to monitor the batch cooling crystallization of (L)-glutamic acid and demonstrated its capability to be able to track the crystallization on-set point and follow the dynamic transition between the α and β polymorphic forms.⁴⁰ We have also developed a multiscale approach for extracting crystal object from raw on-line images.³⁹

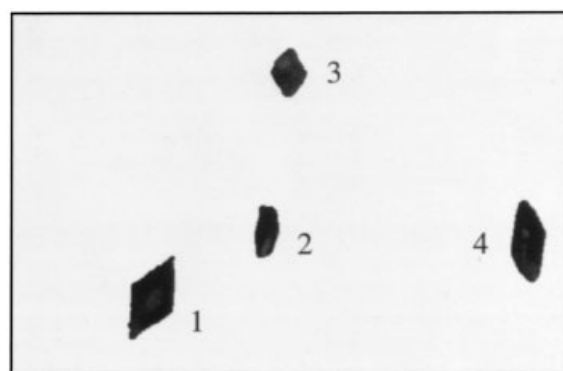
Figure 10 shows four on-line images obtained using the imaging system during a typical batch crystallization experiment together with their segmented images using the image segmentation method reported earlier.³⁹ For the five segmented crystals, descriptors were calculated, and their matching results with the 2-D library are given in Table 1. For each crystal the most similar three images in the library are listed. From the results it can be seen that within the five crystals, two crystals are α form and three are β form.

Figure 11a shows a more complex on-line image containing more crystals. Figure 11b shows the segmented image. The matching results are listed in Table 2, which shows that all four crystals are α form.

In previous work,³⁹ a laboratory particle shape analysis system, the PVS 830,⁵⁵ was also used. Figure 12 shows one of



(a)



(b)

Figure 11. A more complex on-line image of (L)-glutamic acid taken with digital video microscopy system, (a) raw image, and (b) segmented image.

Table 2. The Image Matching Result for the Particle Images in Figure 11

Crystal Number	Retrieved Image Reference	Similarity Distance	Polymorph
1	AlphaM162246	0.82	α
2	AlphaM262146	0.73	α
3	AlphaM064176	1.18	α
4	AlphaM256252	0.33	α

the images obtained from this instrument, which contains three crystals (the one located at edge is ignored). Table 3 lists the matching results.

This case study presents the results and analysis of a number of online crystal images for two forms of (L)-glutamic acid which have been used to test the proposed method, all of which demonstrate that this method gives excellent results. Despite this, we have also found that the method does not give such a good match for some special situations, for example, for small crystal size or when the habit of the crystal changes too much due to the crystal breakage and significant change of the growth environment of the crystals. This problem can in principle be solved through future development of the image library generation system.

Final Remarks

In this article, a new methodology called *camera model* for integrating crystal morphological modeling with *in situ* shape measurement using on-line microscopy is proposed and illustrated by applying it to polymorphic recognition in (L)-glutamic acid cooling crystallization. The integration offers a potentially useful instrument for future crystallization studies, for example, for validation of morphological prediction models, for constructing 3-D shapes from on-line 2-D images, as well as for determination of crystal growth rates of individual facets.

Acknowledgments

This work has been carried out as part of the Chemicals Behaving Badly project funded by EPSRC (GR/R43877, GR/R43860) together with support from an industrial consortium including ANSYS Europe, Ltd., Astra-

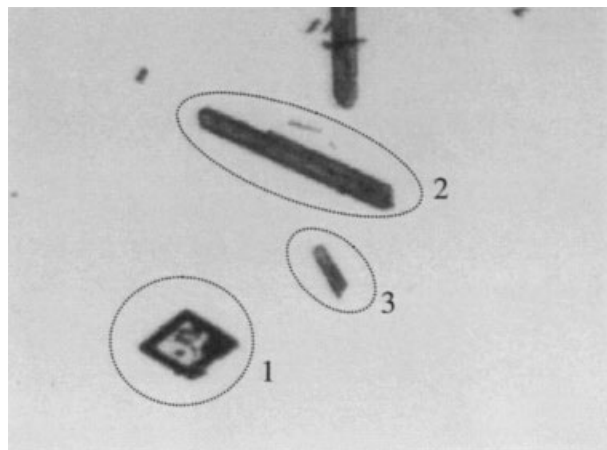


Figure 12. Photomicrograph of (L)-glutamic acid crystals.

Table 3. The Image Matching Result for the Particle Images in Figure 12

Online Images	Retrieved Image Reference	Similarity Distance	Polymorph
	AlphaM344348	0.40	α
	AlphaM164192	0.40	α
	AlphaM158208	0.41	α
	AlphaM334150	0.42	α
	AlphaM154030	0.42	α
	BetaM308296	0.42	β
	BetaM128064	0.52	β
	BetaM276036	0.55	β
	BetaM128244	0.60	β
	BetaM308116	0.67	β
	BetaM058212	2.36	β
	BetaM058032	2.39	β
	BetaM274148	2.45	β
	BetaM096032	2.50	β
	BetaM094212	2.51	β

Zeneca, Bede Scientific Instruments, Ltd., BNFL, Clair Scientific, Ltd., GlaxoSmithKline, HEL, Ltd., Malvern Instruments, Pfizer and Syngenta. The academic partners are Leeds, Heriot Watt and Newcastle Universities. We gratefully acknowledge all these sponsors and all members of this academic/industrial team notably the industrial coordinator L. J. Ford. Special thanks are given to GlaxoSmithKline for providing the imaging system, particularly Kevin Jennings, Mike Wilkinson and Kaz Wood-Kaczmar at GSK for providing technical support with the imaging system, and to Duncan Roberts and David Watson of Malvern Instruments, Ltd. for providing the PVS830 imaging instrument. The corresponding author thanks Malvern Instruments Limited⁵⁵ for sponsoring his readership. J. Calderon De Anda thanks the Council of Science and Technology in Mexico (CONACYT) for providing his PhD scholarship. New research in this direction is being conducted under the support of EPSRC (EP/C009541) and Malvern Instruments Limited.

Literature Cited

- Hartman P, Perdok WG. On the relations between structure and morphology of crystals. *Acta Crystallographica*. 1955;8:49-52.
- Coombs DS, Catlow CRA, Gale JD, Hardy MJ, Saunders MR. Theoretical and experimental investigations on the morphology and pharmaceutical crystals. *J of Pharma Sci*. 2002;91:1652-1658.
- ter Horst JH, Geertman RM, van Rosmalen GM. The effect of solvent on crystal morphology. *J of Crystal Growth*. 2001;230:277-284.
- Docherty R, Roberts KJ. Modeling the morphology of molecular-crystals - application to anthracene, biphenyl and beta-succinic acid. *J of Crystal Growth*. 1988;88:159-168.
- Clydesdale G, Roberts KJ, Lewtas K. Computational modeling study of the growth-morphology of the normal-alkane docosane and its mediation by tailor-made additives. *Molecular Crystals and Liquid Crystals Science and Technology Section a-Molecular Crystals and Liquid Crystals*. 1994;248:243-276.
- Clydesdale G, Roberts KJ, Telfer GB, Grant DJW. Modeling the crystal morphology of alpha-lactose monohydrate. *J of Pharma Sci*. 1997;86:135-141.
- Liu XY, Bennema P. Prediction of the growth morphology of crystals. *J of Crystal Growth*. 1996;166:117-123.
- Clydesdale G, Roberts KJ, Docherty R. Computational studies of the morphology of molecular crystals through solid-state intermolecular force calculations using the atom-atom method. In: Wedlock D, ed. *Colloid and Surface Engineering: Controlled Particle, Droplet and Bubble Formation*. London: Butterworths Heineman; 1993:95-135.
- Clydesdale G, Roberts KJ. Modelling the habit modification of molecular crystals by the action of "tailor-made" additives. In: van der Eerden JP, Bruinsma OSL, eds. *Science and Technology of Crystal*

- Growth*. Dordrecht, The Netherlands: Kluwer academic publishers; 1995:179-192.
10. Clydesdale G, Roberts KJ, Walker EM. The crystal habit of molecular materials: A structural perspective. In: Gavezzotti A, ed. *Theoretical aspects and computer modeling of the molecular solid state*. Chichester: J. Wiley; 1997:203-232.
 11. Clydesdale G, Docherty R, Roberts KJ. Habit - a program for predicting the morphology of molecular-crystals. *Comp Phys Commun*. 1991;64:311-328.
 12. Clydesdale G, Roberts KJ, Docherty R. HABIT95 - A program for predicting the morphology of molecular crystals as a function of the growth environment. *J of Crystal Growth*. 1996;166:78-83.
 13. Accelrys. <http://www.accelrys.com/ceius2/>.
 14. Docherty R, Roberts KJ, Dowty E. Morang - a computer-program designed to aid in the determinations of crystal morphology. *Comp Phys Commun*. 1988;51:423-430.
 15. Clydesdale G, Roberts KJ, Docherty R. Modeling the morphology of molecular-crystals in the presence of disruptive tailor-made Additives. *J of Crystal Growth*. 1994;135:331-340.
 16. Clydesdale G, Roberts KJ, Lewtas K, Docherty R. Modeling the morphology of molecular-crystals in the presence of blocking tailor-made Additives. *J of Crystal Growth*. 1994;141:443-450.
 17. Liu XY, Boek ES, Briels WJ, Bennema P. Prediction of crystal-growth morphology based on structural- analysis of the solid-fluid Interface. *Nature*. 1995;374:342-345.
 18. Winn D, Doherty MF. A new technique for predicting the shape of solution-grown organic crystals. *AIChE J*. 1998;44:2501-2514.
 19. Winn D, Doherty MF. Predicting the shape of organic crystals grown from polar solvents. *Chem Eng Sci*. 2002;57:1805-1813.
 20. Bisker-Leib V, Doherty MF. Modeling the crystal shape of polar organic materials: Prediction of urea crystals grown from polar and nonpolar solvents. *Crystal Growth & Design*. 2001;1:455-461.
 21. Bisker-Leib V, Doherty MF. Modeling crystal shape of polar organic materials: Applications to amino acids. *Crystal Growth & Design*. 2003;3:221-237.
 22. Boerrigter SXM, Cuppen HM, Ristic RI, Sherwood JN, Bennema P, Meekes H. Explanation for the supersaturation-dependent morphology of monoclinic paracetamol. *Crystal Growth & Design*. 2002;2:357-361.
 23. Sweegers C, Boerrigter SXM, Grimbergen RFP et al. Morphology prediction of gibbsite crystals - An explanation for the lozenge-shaped growth morphology. *J of Phys Chem B*. 2002;106:1004-1012.
 24. Liu XY, Bennema P. An inhomogeneous cell model and the growth of crystals. *J of Crystal Growth*. 1996;166:112-116.
 25. Liu XY, Bennema P. Theoretical consideration of the growth morphology of crystals. *Physical Review B*. 1996;53:2314-2325.
 26. Gadewar SB, Doherty MF. A dynamic model for evolution of crystal shape. *J of Crystal Growth*. 2004;267:239-250.
 27. Winn D, Doherty MF. Modeling crystal shapes of organic materials grown from solution. *AIChE J*. 2000;46:1348-1367.
 28. Rohl AL. Computer prediction of crystal morphology. *Current Opinion in Solid State & Mat Sci*. 2003;7:21-26.
 29. Yamamoto H, Matsuyama T, Wada M. Shape distinction of particulate materials by laser diffraction pattern analysis. *Powder Technol*. 2002;122:205-211.
 30. Ma ZH, Merkus HG, Scarlett B. Extending laser diffraction for particle shape characterization: technical aspects and application. *Powder Technol*. 2001;118:180-187.
 31. Mougin P, Wilkinson D, Roberts KJ. In situ measurement of particle size during the crystallization of L-glutamic acid under two polymorphic forms: Influence of crystal habit on ultrasonic attenuation measurements. *Crystal Growth & Design*. 2002;2.
 32. Patience DB, Rawlings JB. Particle-shape monitoring and control in crystallization processes. *AIChE J*. 2001;47:2125-2130.
 33. Patience DB. *Crystal engineering through particle size and shape, monitoring, modeling and control*. University of Wisconsin-Madison; 2002. PhD thesis.
 34. Barrett P, Glennon B. Characterizing the metastable zone width and solubility curve using laser FBRM and PVM. *Chem Eng Res & Design*. 2002;80:799-805.
 35. Barrett P. Selecting in-process particle-size analyzers. *Chem Eng Progr*. 2003;99:26-32.
 36. Barrett P. *In-situ monitoring of crystallization processes*. University College Dublin, Ireland; 2002. PhD thesis.
 37. Li RF, Thomson GB, White G, Calderon De Anda J, Wang XZ, Roberts KJ. Combining morphological modelling and online imaging technique for on-line crystal shape recognition in batch crystallisation processes. *The 7th world congress on chemical engineering*. Glasgow; July, 2005.
 38. Wang XZ, Calderon De Anda J, Roberts KJ, Li RF, Thomson GB, White G. Advances in on-line monitoring and control of the morphological and polymorphic forms of organic crystals grown from solution. *KONA Powder and Particle*; 2005: No 23:69-85. <http://www.kona.or.jp/>.
 39. Calderon De Anda J, Wang XZ, Roberts KJ. Multi-scale segmentation image analysis for the in-process monitoring of particle shape with batch crystallisers. *Chem Eng Sci*. 2005;60:1053-1065.
 40. Calderon De Anda J, Wang XZ, Lai X et al. Real-time product morphology monitoring in crystallization using imaging technique. *AIChE J*. 2005;51:1406-1414.
 41. Calderon De Anda J, Wang XZ, Lai X, Roberts KJ. Classifying organic crystals via in-process image analysis and the use of monitoring charts to follow polymorphic and morphological changes. *J of Process Control*. 2005;15:785-797.
 42. Monisette SL, Almarsson O, Peterson ML. High-throughput crystallization: polymorphs, salts, co-crystals and solvates of pharmaceutical solids. *Advanced Drug Delivery Reviews*. 2004;56:275-300.
 43. Hartley R, Zisserman A. *Multiple view geometry in computer vision*. Cambridge: Cambridge University Press; 2003.
 44. Zhang DS, Lu GJ. Review of shape representation and description techniques. *Pattern Recognition*. 2004;37:1-19.
 45. Lu GJ, Sajjanhar A. Region-based shape representation and similarity measure suitable for content-based image retrieval. *Multimedia Systems*. 1999;7:165-174.
 46. Anquetil PA, Brennan CJH, Marcolli C, Hunter IW. Laser Raman spectroscopic analysis of polymorphic forms in microliter fluid volumes. *J of Pharma Sci*. 2003;92:149-160.
 47. Bernal JD. General discussion on liquid crystal. *Z. Kristallogr*. 1931; 78:363.
 48. Hirokawa S. A new modification of L-glutamic acid and its crystal structure. *Acta Crystallographica*. 1955;8:637-641.
 49. CDS website. <http://cds.dl.ac.uk/>.
 50. Cachesoftware. <http://www.cachesoftware.com/mopac/index.shtml>.
 51. Shapesoftware. <http://www.shapesoftware.com/>.
 52. Wilkinson MJ, Jennings KH, Hardy M. Non-invasive video imaging for interrogating pharmaceutical crystallization processes. *Microscopy Microanal*. 2000;6:996-997.
 53. Wilkinson MJ, Jennings KH, Plant R, Logan R, Drayson B. Particle size and shape measured for process monitoring using high-speed image analysis. In: *Particulate Systems Analysis*. Harrogate, U.K.; 2003.
 54. IO-Industries. <http://www.ioindustries.com/>.
 55. Malvern Instruments, Ltd. Webpage. <http://www.malvern.co.uk>.

Manuscript received Jan. 21, 2005, and revision received Jan. 19, 2006.